The Use of Dam Break Model to Simulate Tsunami Run-up and Scouring Around a Vertical Cylinder

Kuswandi[1] and R. Triatmadja[2†]

[1] *Department of Civil Engineering Faculty of Civil Engineering and Planning, Institut Teknologi Medan, North Sumatra, Indonesia*

[2] *Department of Civil and Environmental Engineering, Faculty of Engineering, Universitas Gadjah Mada, Indonesia*

† *Corresponding Author Email: radianta@ugm.ac.id*

ABSTRACT

This research paper deals with the use of a dam break system to generate a surge model to study tsunami run-up, run-down and scouring around a vertical cylinder. The dam break system was provided with one or two gates to store water at a predefined depth; the water could then be quickly released by opening the gates to create a tsunami surge that runs up on land. In addition, numerical simulations of dam break surges resulting from various lengths of reservoirs were conducted to obtain more findings for further analysis regarding the characteristics of the dam break surges. A vertical cylinder model was installed on the beach at 6 meter downstream of the main gate to study the scour caused by the tsunami surge. The bed material was fine sand with a 0.19 mm diameter. The results were compared with existing experimental results. The comparison indicated that the dam break surge can be used to simulate tsunami surges by adjusting the reservoir length, the reservoir depth and the water depth downstream of the gate. The ratio of the difference between the upstream and downstream water depth on one side to the length of the reservoir on the other affect the run-up height and duration. Thus, this ratio should be considered when simulating tsunami based on dam break systems. Although different in magnitude, the shape of both the surge mareogram and the velocity time history of the tsunami surge generated using dam break system was comparable with the tsunami surge induced by a solitary wave generated using a long flume. For the relatively large cylinder located at the bore location, the separation flow was strongly directed to the wall which produced significantly unsymmetrical scour result.

Keywords: Dam break; Run up; Run down; Tsunami; Scour; Simulation.

NOMENCLATURE

B	flume width	R_u	run-up height
b	cylinder diameter	r	distance
C^+	positive surge	t	time
C^-	negative surge	V	velocity
d	water depth at arbitrary time	V_e	experimental surge velocity
d_s	scour depth	V_k	velocity from Kato's experiment
d_0	initial water depth at the reservoir	V_{emax}	maximum experimental surge velocity
d_3	downstream initial water depth	W	width of dislocation
d_{50}	grain size diameter		
d_{max}	maximum water depth	ρ_s	density of sand
d'	$d_0 - d_3$	ρ	density of water
d''	4/9 d'	ω	average fall velocity
g	gravitational acceleration	υ_0	kinematic viscosity
H	surge height	ξ	$\frac{(d_0 - d_3)}{L}$
h	water depth		
L	reservoir length or dislocation length	ζ	$\frac{R_u}{\frac{4}{9}(d_0 - d_3)}$
n	porosity		
P	pressure		

1. INTRODUCTION

A tsunami model requires a fairly long flume to simulate the tsunami accurately. Even a flume of 135 m, as used by Kato *et al.* (2000) and Tonkin *et al.* (2003), may only simulate a relatively small and short tsunami represented by a solitary wave. This is because the length of a tsunami, once generated, is equal or slightly larger than the size of the dislocation area, as shown by Table 1. The table indicates that a model scale based on the Froude similarity should at least be 1:1000 to represent a tsunami with a length of 150 km in a flume of 150 m. Such a long flume facility is rarely available. Even if the length of the flume is sufficient, the height of the tsunami is too small when scaled down by 1000. The model scale is insufficient when simulating sediment transport and scouring due to a tsunami.

A dam break surge model in a short flume was used here to represent a tsunami attack on land. The simulations did not require a long flume, since the tsunami propagation process was omitted in the simulation. The dam break was represented by a quickly opened gate that originally divided the flume into a reservoir (the sea) and a beach model. With such a mechanism, the maximum ratio of scour depth around a cylindrical column to surge height (d_s/H) was 0.4 (Triatmadja *et al.*, 2011). There were limitations due to using only one gate that represented the dam break (one-gate system). These limitations are that the length of the surge crest that depends on the length of the reservoir and the surge slope that cannot be adjusted to simulate different shapes of tsunamis. These properties can be adjusted in a two-gate dam break system, as depicted in Fig. 1. The gates may be opened simultaneously or at slightly different times. The simulation of the dam break surge with two gates, set both upstream and downstream from the water body may represent the surge of a tsunami more appropriately. The negative and positive surges, with a celerity of either C^+ or C^- when the gates are opened, are depicted in Fig. 1. The dotted lines indicate the situation when the gates are opened simultaneously. In this case, the negative surge from the left meets the positive surge from the right side at the middle of the reservoir.
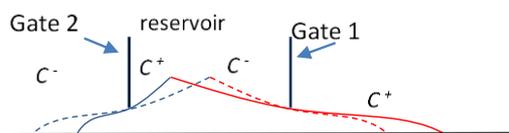
Fig. 1. Sketch of dam break surge in a two-gate dam break system with different opening times.

Since the celerity *C* and the shape of the surges are symmetrical, the surge condition is similar to that of a dam break with one gate but only half of the reservoir length. The solid lines indicate the surge's condition when the left gate is opened shortly after the right gate. The timing of the gates opening may create a varying dam break surge that represents tsunami of different slopes and lengths.

Another problem with the simulation of tsunami surge based on a dam break surge is that the downstream surge may be reflected by the downstream end of the flume, while the negative wave could be reflected by the upstream end of the flume. If the water were drained to the ground tank by opening Gate 2, the reflection after the run-down and the secondary run-up would be significantly altered. A significantly smaller run-up could still exist, depending on how fast the water is drained. If this run-up exists, it would be easier to control. When necessary, an additional gate (third gate) can be provided to stop the unwanted secondary run-up due to reflection.

Scouring due to a tsunami has been identified as an important aspect that has to be dealt with to assure safer constructions with regards tsunami damage. Levee structures, seawalls, and housing with shallow foundations have collapsed during tsunami due to scouring. Dalrymple and Krieble (2005) showed examples of such damage. Even a relatively small tsunami run-up may scour and damage lightly reinforced piling and pedestal foundations (Francis, 2006). Although a tsunami attack may last only several minutes, the attack can result in a maximum scour depth that is dictated mostly by the natural slope stability of the bed material.

The characteristics of tsunami run up on land, either as broken or non-broken waves, are important parts of tsunami simulations because they govern the interaction between tsunami surge and the structures on land. The scouring mechanism around a vertical cylinder is affected by the speed of the surge and the duration of the run-up and run-down. They depend on the surge height, the surge length, and the slope of the land. This signifies that simulating tsunami-induced scouring around a structure requires similarities in tsunami characteristics such as tsunami height, run up, run down, surge velocity, and the duration of the process. Such similarities require a very long and large wave flume. Therefore it is important to study the applicability of a dam break model in a short flume to simulate tsunami run-up, run-down, and the possibility to simulate local scouring. When the use of relatively short flume for dam break model can be justified, further research on tsunami run-up, run-down, scouring and other related tsunami simulation can be conducted using a relatively short flume.

This research is aimed at the use of a dam break system to simulate tsunami run-up and run-down by reducing or eliminating the problem of secondary run-up that is generated by wave reflection from the upstream wall of the flume. The elimination of the secondary run-up is expected to enable better observation of the run-down. The study also aims to find the relation between the run-up and the water depth for both upstream and downstream from the main gate (Gate 1 in Fig. 2) and the length of the reservoir (distance between Gate 1 and Gate 2). The finding is expected to be a useful guide for similar research, since the available analytical approaches and experiments on dam break surges use relatively long flumes (much longer than the water depth) in

Table 1 Example of bottom dislocation sizes and water depth at tsunami source

Location	Date	L (km)	W (km)	Range of Water Depths (km*)
Aceh, Indonesia (Wang and Liu, 2006); Vallée (2007)	26 Dec 2004	500	150	0 - 5
East Japan, (Mas *et al.*, 2012)	11 March 2011	500	>100	0 - 5
Pangandaran, Indonesia (Kongko, 2011)	17 June 2006	200-375	80-150	2-7

* Ranges estimated by authors based on Google Earth© elevation.

Notation;
1. Open channel (20,7 x 1,43 x 1,50 m)
2. Beach slope 1:20 (use sand material)
3. Reservoir
4. Vertical cylinder
5. Dam break mechanism
6. Handle for open gates
7. Gate-1
8. Gate-2
9. Gate-3
10. Pump and plumbing system
11. Drainage hole
12. Drainage channel

Hydraulic cycles;
i.   run-up direction
ii. run-down direction
iii. Flow direction from Gate-1
iv. Flow to drainage channel
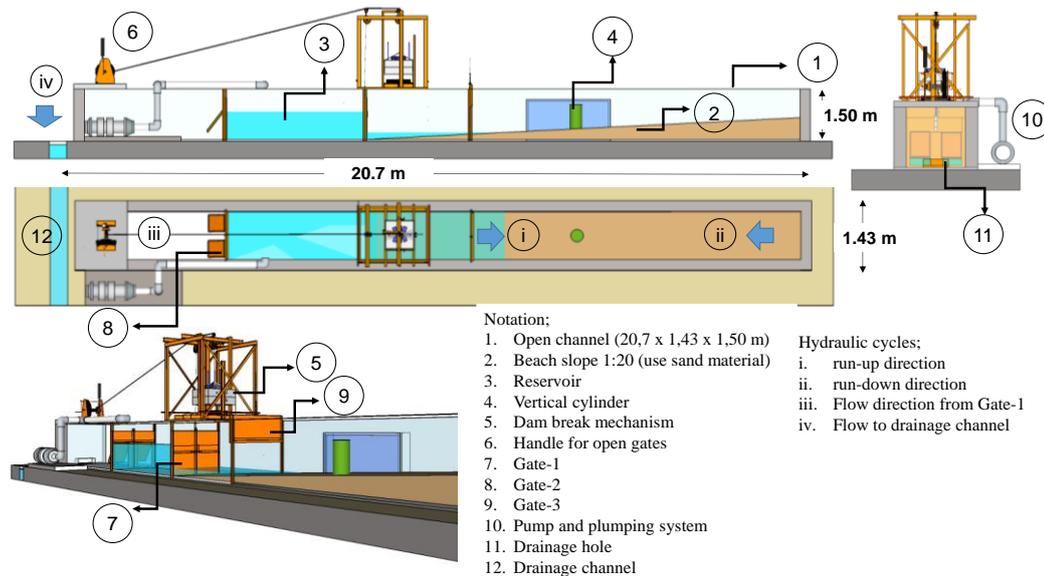
Fig. 2. Physical model experimental layout.

which the flow can be considered to be shallow water. The study of scouring around a vertical cylinder was meant to indicate the ability of the facility to simulate tsunami scour around a cylinder at the shoreline.

2. MATERIALS AND METHODS

2.1. Physical Model Simulation

A limited length flume was utilized to generate a tsunami surge that would run-up on land. The length and the width of the flume were 20.7 m and 1.43 m respectively (Fig. 2). The surge was represented by a dam break surge by the control of both the upstream and downstream water depths. The dam was represented by a gate (Gate 1), which was located 8 m from the upstream end of the flume, as in Triatmadja and Nurhasanah (2012). A second gate (Gate 2) was installed 4 m upstream of Gate 1. The area between Gate 1 and Gate 2 is called the reservoir, where the distance between the gates represents the length of the reservoir or the length of the dislocation. The length of the reservoir can be adjusted to meet the requirements of the simulated tsunami surge by adjusting the location of Gate 2. The initial depths at the reservoir (between Gate 1 and Gate 2) and downstream of Gate 1 were designated as d_0 and d_3 respectively, while d' represents the difference between d_0 and d_3. The water depth at an arbitrary time and space

downstream of Gate 1 is defined as d. When the gates were opened, the water rushed downstream of Gate 1 as surge front, while Gate 2 allowed the water to flow into a ground tank. A third gate was installed downstream of Gate 1 to protect against reflection from the upstream water after the run-up, as this could create a second, unwanted run-up. The third gate was closed as soon as the run-down reached Gate 1. Theoretically, when the gates were opened, the maximum water height downstream of Gate 1 above the initial water level (d_3) was 4/9 d' (see for example Chanson, 2005). This value (4/9 d') is considered to be the wave height in this study. In addition to the physical simulations, numerical simulations were conducted with varying water depths and lengths of the reservoir to simulate run-ups.

The experiment for scour observation was set up similarly to that of the simulations of Kato *et al.* (2000) and Tonkin *et al.* (2003), particularly with regard to the limitation of the flume size. A concrete vertical cylinder was installed 6 m downstream of Gate 1. The vertical cylinder was approximately 2 m downstream of the shoreline, while the vertical cylinder position in Kato *et al.* (2000) and Tonkin *et al.* (2003) that was used for comparison was at the coast line. The diameter of the vertical cylinder was 0.357 m, such that the relative diameter (ratio between the cylinder diameter and the width of the flume) equaled 0.25, as in Kato *et al.* (2000) and
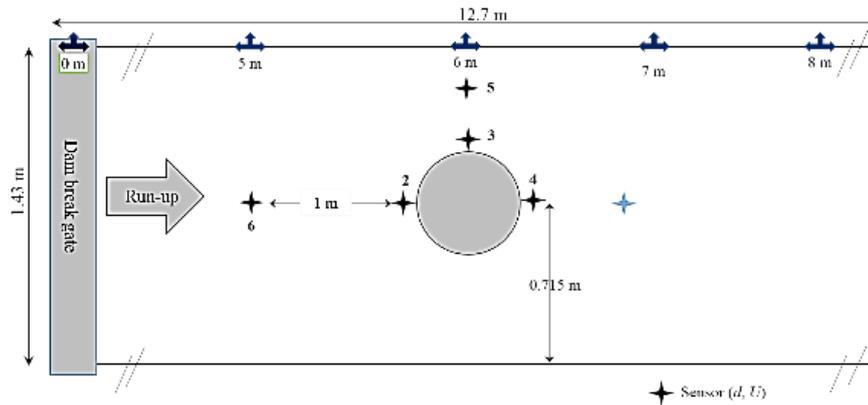
Fig. 3. Detailed layout of measurement stations around the vertical cylinder model.

Tonkin *et al*. (2003). Four wave recorders were installed at similar positions (relative to the vertical cylinder), as with those of Kato *et al*. (2000) and Tonkin *et al*. (2003). The wave height (d') was made as large as possible as long as the run-up did not reach the downstream end of the flume. The experimental lay out is given in Fig. 2.

The water depth and flow velocity were measured using tilting sensors at Station 1, 2, 3, and 4 simultaneously. The sensor measured the water velocity based on the strain gauge voltage signal, which depends on the tilting degree of the sensor. For this, a higher velocity means a higher tilting degree and voltage. The sensors were calibrated using a steady flow along an open channel before the experiment was conducted. Station 5 was used to measure the water depth and was especially aimed at comparing the water depth during simulations with various vertical cylinder diameters. The difference of the water depth at this station (beside the vertical cylinder) was expected to indicate whether the cylinder size significantly reduced the flow width, created a reflection, and affected the flow depth. The detail layout of the measurement stations is given in Fig. 3.

The bed of the flume that started from the downstream end and ended 1 m downstream of Gate 1 was made of fine sand and was erodible. From 1 m downstream of Gate 1 up to the upstream end of the flume, the floor was a fixed bed. Before each test, any change to the bed material, including scouring resulting from the previous test, was reshaped to form the intended slope of 1: 20, starting from the Gate 1 position and ending at the downstream end of the flume. The bed surface elevation around the vertical cylinder model was measured using a laser distance meter before and after each test. The bed surface elevation measurement was conducted every 1 cm in both the X-axis and Y-axis directions. The vertical accuracy of the distance was approximately 1 mm. Before the test, water was pumped into the flume in between Gate 1 and Gate 2, up to a level where the upstream depth equaled d_0. Water was also pump into the downstream area up to the level where the downstream depth equaled d_3.

The bed material for the experiment was collected

from sand dunes at Parangtritis Beach in Yogyakarta, Indonesia. The dunes were created by wind energy that lifts up fine sand and drops it when the wind energy is reduced. Therefore, the sand particles collected at the top of the sand dune were expected to be fine, with no need for sieving. The properties are given in Table 2. The material has also been used by Kuswandi *et al*. (2017).

Table 2 Properties of the bed material

diameter (d_{50})	0.19 mm
ρ_s	1.76 ton/m^3
Porosity (n)	0.45
average fall velocity (ω)	4.9 cm/s

2.2. Numerical Simulations

Numerical simulations were conducted in addition to the physical model simulations. This is because numerical simulations are more efficient and faster than physical model simulations. The simulations were conducted using DualSPHysics, which is open source software developed by Crespo *et al*. (2015). DualSPHysics is based on the Navier Stokes Equation, which is capable of simulating very complicated flow problems. The earlier version of the coding (SPHysics) was tested for simulating dam breaks over wet beds by Crespo *et al*. (2008), which validated the use of the software for similar tasks. Dal *et al*. (2017) suggested that DualSPHysics is a useful tool for simulating dam break model. Aureli *et al*. (2015) suggested that a three-dimensional (3D) simulation using SPH is able to accurately simulate the dam break wave force on a wall structure. Xu (2016) suggested that the SPH method is accurate and stable for modelling a 3D free-surface flow with large deformation as in the dam break flow. The above references suggest that DualSPHysics, which is based on SPH and has been widely used, is an appropriate tool for this study.

DualSPHysics and its predecessor were based on Smooth Particle Hydrodynamic (SPH) numerical modeling, which was originally developed by Lucy (1977). Unlike the usual differential equations, solved using finite difference or finite element

methods, the SPH describes the domain of computation using arbitrarily unconnected particles and solves the field function with the integral representation method. Such integration is replaced by summation over the corresponding values of the neighboring particles in a local area of computation (Liu and Liu, 2003). The implementation of the method for the DualSPHysics program is explained in Crespo et al. (2008) and Crespo et al. (2015) as follows:

A function *F(r)* can be interpolated by

$$F(r) = \int F(r') W (r_a - r_b, h) dr' \qquad (1)$$

In which $W(r_a - r_b, h)$, written as W_{ab}, is the weighting function, *h* is smoothing length, and *r* is the distance between particles *a* and *b*. In a discrete approach this leads to the following:

$$F(r) = \sum_b F(r_b) \frac{m_b}{\rho_b} W_{ab} \qquad (2)$$

Subscripts *a* and *b* indicate the particles in consideration, while *m* and ρ indicate their mass and density respectively. There are a number of weighting functions; one of them is the cubic spline, which was developed by Monaghan and Lattanzio (1985) as the following equation:

$$W_{ab} = \frac{1}{\pi h^3} \begin{cases} 1 - \frac{3}{2}q^2 + \frac{3}{4}q^3 & if \ 0 \le q \le 1 \\ \frac{1}{4}(2-q)^3 & if \ 1 \le q \le 2 \\ 0 & otherwise \end{cases} \qquad (3)$$

Where *q = r/h*.

The above weighting function can be shown in a graphic, as in Fig. 4.
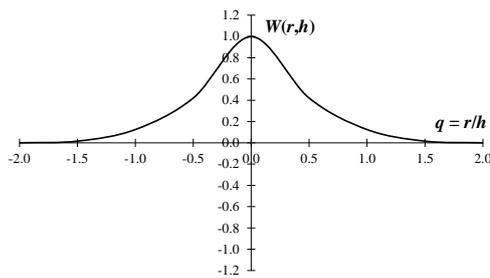
Fig. 4. Cubic spline weighting function.

The larger the smoothing function, the larger the number of particles involved in the equation, which also makes the solution smoother. Since the computation domain is represented by particles, the results are more accurate the smaller the particle is, but this carries the cost of increased computation time.

The momentum equation is written as follows:

$$\frac{dv}{dt} = -\frac{1}{\rho}\nabla P + g + \Gamma \qquad (4)$$

The last term on the right-hand side of the equation represents the dissipative term. DualSPHysics offers artificial viscosity, laminar viscosity, and sub-particle turbulence for the dissipative term.

For example, the momentum equation with artificial viscosity (Crespo et al., 2015) reads as follows:

$$\frac{dv_a}{dt} = -\sum_b m_b \left(\frac{P_b}{\rho_b^2} + \frac{P_a}{\rho_a^2} + \Pi_{ab} \right) \nabla_a W_{ab} + g \qquad (5)$$

Where *P* is the pressure associated with the corresponding particle, v_0 is kinematic viscosity and

$$\Pi_{ab} = \begin{cases} \dfrac{-\alpha \overline{C_{ab}}\ \mu_{ab}}{\overline{\rho_{ab}}} & v_{ab}.r_{ab} < 0 \\ 0 & v_{ab}.r_{ab} > 0 \end{cases} \qquad (6)$$

Here, $r_{ab} = r_a - r_b$ and $v_{ab} = v_a - v_b$, while *r* and *v* represent the position of the particles and its velocity respectively, $\overline{C_{ab}}$ is the mean speed of sound of *a* and *b*, $\mu_{ab} = hv_{ab}.\frac{r_{ab}}{r_{ab}^2 + 0.01h^2}$, and *a* should be tuned to obtain the proper dissipation.

The continuity equation is written as in Crespo et al. (2015):

$$\frac{d\rho_a}{dt} = \sum_b m_b v_{ab} . \nabla_a W_b \qquad (7)$$

Similar to all other numerical models, DualSPHysics requires proper boundary conditions and time steps. Further details of the discrete equations and their solutions can be found in Crespo et al. (2015).

Since the solutions of the equations dealt with each of the particles and the surrounding particles within the region of influence with radius *r =2 h* based on the weighting function, the computation is tedious. DualSPHysics uses both CPU and GPU for the iteration, which makes it faster than its predecessor that uses only the CPU.

Table 3 Physical model experiment (L = 4 m, Slope 1: 20)

d_0 (m)	d_3 (m)	One gate	Two gates
0.5	0.48	Yes	Yes
0.5	0.45	Yes	Yes
0.5	0.40	Yes	Yes
0.5	0.38	Yes	Yes
0.5	0.35	Yes	Yes
0.5	0.30	Yes	Yes
0.5	0.20	Yes	Yes
0.5	0.00	Yes	No
0.45	0.00	Yes	No
0.55	0.00	Yes	No

3. RESULTS AND DISCUSSION

The scenario of the physical model regarding the water depth in the reservoir (d_0) and at the downstream side (d_3) was given in Table 3, together with test conditions of both a two-gate dam break and
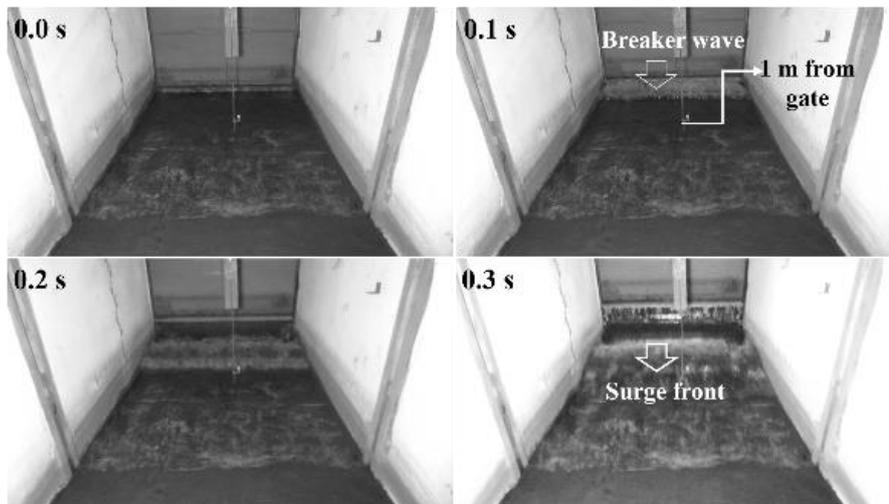
Fig. 5. The surge on initially dry bed at $d_0 = 0.50$ m.
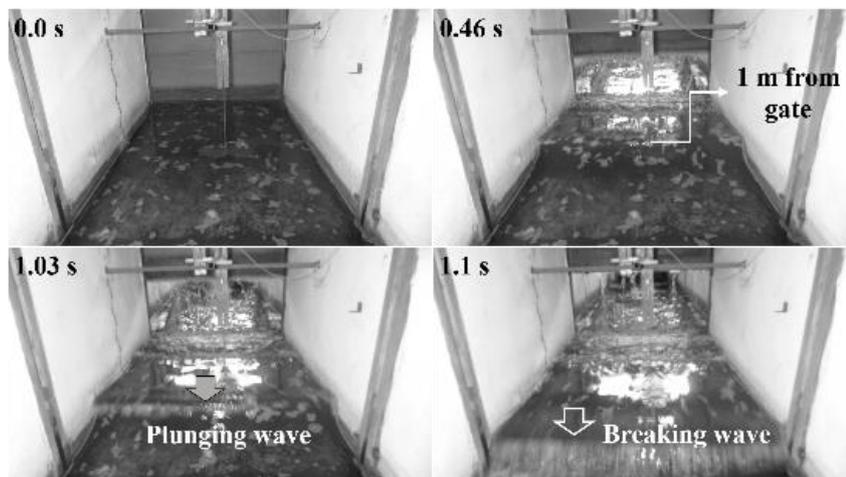
Fig. 6. Evolution the surge on initially wet or inundated area with $d_0 = 0.50$ m, $d_3 = 0.2$ m and $d' = 0.3$ m. The time was measured starting from gate opening.

one-gate dam break system. The reservoir length and beach slope for all experiments were 4 m and 1: 20 respectively.

Both gates in two-gate dam break simulations were opened simultaneously.

3.1 Physical Model Surge Front

Figure 5 shows the propagation of a tsunami-like surge generated by the dam break system on a dry bed where $d_0 = 0.50$ m. Once the gate was opened, the surge front formed a bore, which quickly propagated downstream. The surge front have reached 1 m from the gate location approximately 0.3 s after the gate was opened.

Figure 6 shows the evolution of the tsunami's surge on an initially wet downstream area. The water surface downstream of the gate increased after the gate was opened and created unbroken wave. The shape of the wave can be observed at Fig. 6 at time 0.46 s. The wave started to plunge at 1.5 m downstream from the gate's position as can be seen

in Fig. 6 (at 1.03 s).

The wave broke at 2 m from the shoreline, 1.1 s from the time when the gate was opened. This indicates that the generated wave model that used the dam break system with a downstream initial inundation was similar to the tsunami that propagated and broke at the shallow water with fully developed surges. Figure 7 offers a better view of the wave forms at Station 6, which was located at 5 m from Gate 1. The waves did not become a bore but was highly asymmetric where the front was steep, depending on the d'. All the simulated surges became bores before reaching the vertical cylinder at 6 m from Gate 1.

3.2 Physical Model Tsunami Mareogram

The tsunami mareogram at Station 2 for the one-gate and the two-gate dam break systems is provided in Fig. 8. The time axis for all the surges was set so that they reached Station 2 at the same time. Station 2 was located 0.5 cm in front of the cylinder directly facing the surge. Thus, water increased significantly for a short time when the surge hit the vertical cylinder.
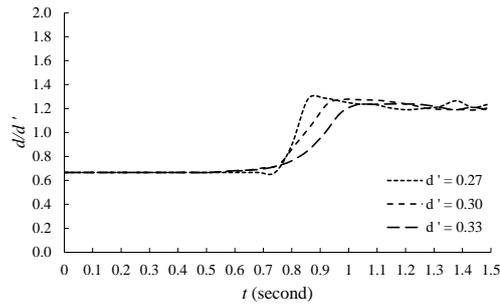
Fig. 7. Surge front on an initially wet or inundated area measured at Station 6. The starting time of the recording was not the same as the time of gate opening.
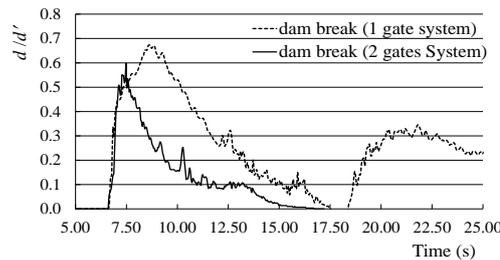
Fig. 8. An example of surge mareogram (d_0 = 0.5 m, d_3 = 0.2 m).

It can be seen in Fig. 8 that there was a reflection following the first run-up when the dam break was simulated using one-gate dam break system. Such a reflection created a significant secondary run-up in front of the vertical cylinder (Station 2). On the other hand, the two-gate dam break system produced a less significant reflection that could be stopped using the third gate prior to the secondary run-up when necessary. It may be said that the two-gate dam break system can be used to modify the length of the reservoir and to reduce the secondary run-up.

It is interesting to compare the present simulation with that of Kato *et al.* (2000), although they used a much longer flume and simulated the tsunami using a solitary wave and despite the fact that the position of the vertical cylinder and the station of observation were slightly different, as described in Section 3. Figure 9 shows the difference between the surge shape of the present experiment and that of Kato *et al.* (2000), where the present relative surge height (d/d') was multiplied by 4.5. This multiplier was selected so that the maximum value of d/d' for the present experiment would be approximately equal to the maximum value of d/H for Kato *et al.* (2000). As can be inferred from Fig. 9, the shape of the dam break surge resulting from the two-gate dam break system and that of Kato *et al.* (2000) are somehow similar, as indicated by the relatively small difference. On the other hand, the surge of the one-gate dam break system is shown to have a longer peak duration and a significantly longer time needed to reach the peak. The shorter peak duration of the two-gate dam break system was mainly because the water was drained through the downstream gate of the reservoir and hence represented, in this case, a half-length of the one-gate system flume. The mean

and standard deviation of relative residuals (4.5 d/d' - d/H)/d_{max}), starting from the surge arrivals to the end of the run-down time (17 s), are 8% and 9% for two-gate dam break system and 19% and 22% for the one-gate dam break system respectively. This indicates that the length of the reservoir is an important factor for reproducing the tsunami surge.
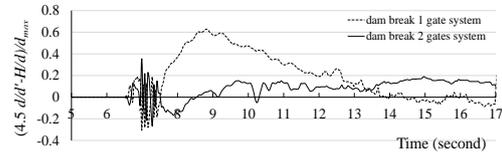
Fig. 9. Relative shape difference between the dam break surge of the one- and two-gate dam break system and that of Kato *et al.* (2000) measured at Station 2, d_0 = 0.5 m, and d_3= 0.2 m. The relative surge height of the present experiment was multiplied by 4.5. d/H is the relative surge depth as in Kato *et al.* (2000).

3.3 Physical Model Run-up Height

The run-up height is defined as the vertical distance between the initial water level at the beach (downstream of Gate 1) and the maximum water elevation on land. Synolakis (1987) indicated that the run-up height of solitary wave depends on wave height, water depth, and slope.

It was found that the run-up depended on both the basin depth (d_0) and the downstream depth (d_3). The run-ups are comparable with those of solitary waves on similar slope (Synolakis, 1987) when H/d <0.1 (Fig. 10). As the wave started breaking, the present experiment resulted in relatively higher run-ups.
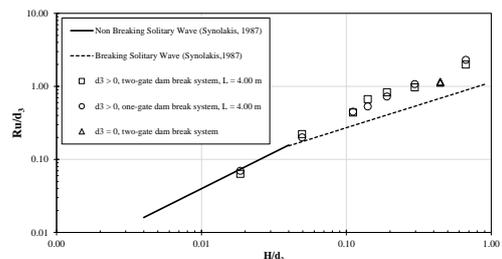
Fig. 10. Surge run-ups of the present experiment as compared with those from Synolakis (1987).

Figure 10 indicates that, as H/d_3 increases, the difference of R_u/d_3, measuring between the dam break surge run-up and the solitary run-up, becomes higher. When H/d_3< 2%, the dam break surge run-up is similar to that of a solitary wave. The two-gate dam break system with a 4 m reservoir length produced a run-up height similar to that of the one-gate dam break system of the same length. This means that, for such a reservoir length (2.00 m up to 4.00 m) the model run-up heights were not significantly affected by the reservoir length. Figure 10 can be used to approximate the length of the reservoir when the run-up height of dam break wave similar to solitary wave is required by adjusting the

value of L, d_0 and H. Based on the shallow water equation and a flatbed dam break situation, Chanson (2005) showed that the maximum run-up height of a dam break on a dry, frictionless sloping beach is $2d_0$. The finding is certainly valid when the reservoir is long enough to generate a long wave. A very short flume may produce short waves relative to the water depth. For a short wave, the wave energy moves slower than the wave celerity, and thus some of the energy will be left behind to generate new waves. The short waves, therefore, do not use all of their energy and thus produce a lower run-up. To study the effect of reservoir length on run-up height, numerical simulations were conducted.

3.4 Numerical Model Results

The scenario of the numerical simulations using DualSPHysics is given in Table 4. The depth of the reservoir was set at a maximum of $d_0 = 0.50$ m for a better scale and so that the length of the run-up could still be accommodated by the flume.

Table 4 Numerical model scenario (L = 0.25 m, 0.50 m, 1.00 m, and 2.00 m, slope 1: 20, One-gate system)

d_0 (m)	d_3 (m)
0.5	0.35
0.5	0.30
0.5	0.25
0.5	0.20

The results of the numerical models are given in Fig. 11, together with the results from physical model experiments. When the length of the reservoir was 4 m, the numerical model results were very close to the experimental results.
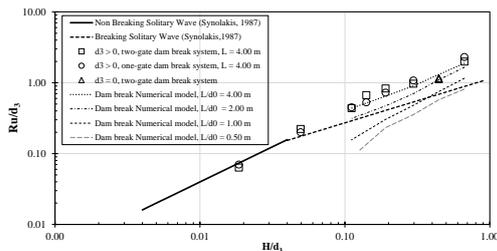
Fig. 11. Surge run-ups of the numerical model as compared with those from the present physical model and Synolakis (1987).

Such an agreement indicated that the accuracy of the numerical simulation was verified. As the length of the reservoir was reduced, the numerical model resulted in a lower R_u/d_3. It can be seen clearly in Fig. 11 that the length of the reservoir relative to the reservoir depth (L/d_3) and H/d_3 significantly affects the run up heights. As stated previously, the short waves (created by the short reservoir) do not retain energy as they travel but instead leave some portion of it behind them. Other than that, a short flume with a large water depth downstream provides a longer space for the dam break wave to travel before

reaching the shore. As the wave travels, the numerical dissipation reduces the wave energy or the wave height (Panalaran *et al.*, 2016).

Figure 12 shows the dam break wave for $L = 2.00$ m and $L = 0.50$ m, where $d_0 = 0.50$ m and $d_3 = 0.40$ m. The number of waves that were created is not very clear, but it can be seen that, with $L = 2.00$ m, the wave moved faster than with $L = 0.50$ m. After 8.5 s, the dam break wave with $L = 0.50$ m traveled approximately 6.25 m, while the dam break wave with $L = 2.00$ m traveled approximately 7.75 m and its run-up had already begun.
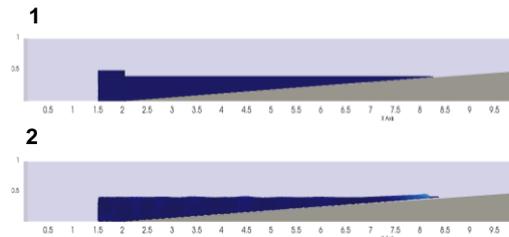
a. $L = 0.50$ m, $d_0 = 0.50$ m, $d_3 = 0.40$m
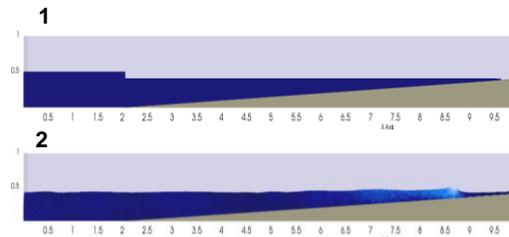
b. $L = 2.00$ m, $d_0 = 0.50$ m, $d_3 = 0.40$m
Fig. 12. Numerical dam break waves propagation using DualSPHysics. (1) Initial condition, (2) After 8.50 s.

The lower speed of the wave front for $L = 0.50$ m, indicated the larger amount of energy that was left behind by the first wave front. As can also be seen in Fig. 12, the front of the dam break wave with $L = 2.00$ m was higher and also at a higher speed, as indicated by brighter color. The higher wave front and speed were responsible for the higher run-up.

It is interesting to present the run-up height against the reservoir length to indicate the effect of reservoir length on run-up in Fig. 13.
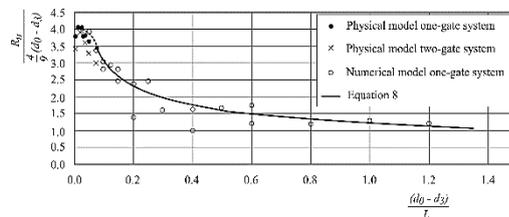
Fig. 13. Run-up height as a function of d_0, d_3, and L.

The best fit line of the data can be approximated as follows:

$$\zeta = 1.22\xi^{-0.4} \qquad (8)$$

where $\xi = \dfrac{(d_0 - d_3)}{L}$ and $\zeta = \dfrac{R_u}{\dfrac{4}{9}(d_0 - d_3)}$.

In Fig. 13, when $d_3 = 0$ and for a significantly large L, we see that the value of R_u is approximately $2d_0$. In fact this is the maximum value of the run-up, as indicated by Chanson (2005). The dash line in Fig. 13 is an approximate extrapolation line of fit when ξ close to zero in which $\zeta = 4$. Figure 13 and Eq. (8) can be used to design the length of the reservoir model to achieve the required run up height relative to the wave height, based on d_0 and d_3. It has to be noted that L/d_0 should not be relatively small, as the dam break wave will be strongly dispersive, and Eq. (8) may not be applicable any longer. Figure 13 suggests that the results from $L/d_0 = 4$ (at $d_0 = 0.5$ m and $L = 4$ m in the two-gate system) were almost exactly the same compared to the results from $L/d_0 = 8$ (at $d_0 = 0.5$ m and $L = 4$ m in the one-gate system). Thus, the run-up may not be significantly different for $L/d_0 = 4$.

In a real tsunami event near the coast line, the value of ξ is normally very small, since the tsunami length is significantly larger than the water depth. For a tsunami that is generated by a dislocation of a width of 100 km at a 6000 m water depth, the length and the speed of the tsunami will be around 100 km and 873 km/h respectively. The duration for traveling the total tsunami length is 412 s. Assuming that this duration does not change, as in the sinusoidal wave period, the length of the tsunami at a depth of 10 m (near the coastline) becomes 4082 m, much more than 40 times of the water depth. Hence, tsunami run-up may be more similar to the dam break condition rather than the condition of a solitary wave.

3.5   Physical Model Run-up and Run-down Speed

The tilting sensor produced a positive velocity during the run up and a negative velocity during the run down. The result of the experiment is plotted in Fig. 14. The maximum velocity (2.5 m/s) was reached at the surge front and declined rapidly during the run up. In fact, the run-up only lasted for approximately 2.5 s and was followed by the run down process. The run up and run down velocities were compared with that of Kato *et al.* (2000) in Fig. 13, where the time has been adjusted so that the surge fronts of both experiments started at the same time. Please note that it was the relative difference in speed between the present velocity (V_e) and that of Kato (V_k) to the present velocity that was plotted in Fig. 13. In general, the shape of the flow velocity curves (velocity against time) during the run up and the run down were similar. However, the present experiment indicated a higher maximum run up speed within approximately 0.75 s, after which the present experiment under predicted that of Kato *et al.* (2000). This was partly because, in the present experiment, the wave was of a surge type or bore. It seems that, in Kato *et al.* (2000), the measurement was conducted at a position prior to the bore formation, and thus, even with a higher wave, the flow speed was significantly lower than in the present

simulation.
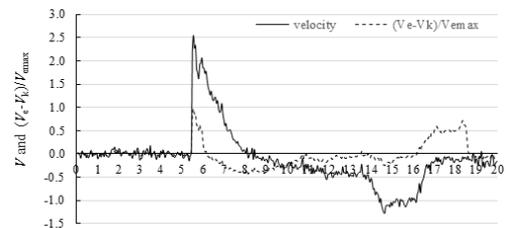
Fig. 14. Run-up (positive value) and run-down (negative value) velocities of the present experiment (V_e) and that of Kato *et al.* (2000) experiment (V_k).

At the end of the run-down time (16.2 s to 18.8 s), the relative difference of the flow speed was significantly large. This indicated that the run-down time of the present experiment was 2.6 s shorter than that of Kato *et al.* (2000).

3.6   Physical Model of Scouring Around a Vertical Cylinder

The run-up and run-down flow resulted in scouring around the vertical cylinder model. During the run up, the bed around the vertical cylinder was highly scoured, especially during the flow with a high Froude number at the surge front. Near the end of the run-up, the flow speed diminished, as can be seen in Fig. 14. For approximately 6 s (starting from 8 s to 14 s), the run down flow was quite slow, where sediment could have been redeposited at the scouring location and subsequently reduced the scour depth. In this research, only the final results of the scouring were observed, as given in Fig. 15. The scour pattern for $b/B = 0.25$ indicated that the scour mostly happened at the sides of the vertical cylinder (Fig. 15(a) and Fig. 16(a)). There was small or negligible local scouring in front and at the rear of the vertical cylinder, as can be seen in Fig. 15(a) and Fig. 16(b). The maximum scour depth was 0.0352 m or 0.264 d'', where $d'' = 4/9$ d'. The maximum depth and the scour pattern were significantly different compared to that of Tonkin *et al.* (2003). In Tonkin *et al.* (2003), the scour pattern was almost symmetrical around the vertical cylinder, while the maximum scour depth was 0.52 H, twice of the present result. This was likely due to a slightly different cylinder location, the effect of the cylinders' relative sizes, and a slightly different bed material, in addition to the velocity difference depicted in Fig. 14. In the present experiment, the vertical cylinder was located where the tsunami had become a bore with significantly high Froude number. With a higher Froude number, the flow separation was stronger where the flow was more directed to and ultimately reflected by the walls. The reflections produced a higher water level near the cylinder, which subsequently reduced the flow speed.

Using the same experimental method, Kuswandi *et al.* (2017) found that the scour pattern around the vertical cylinder where $b/B = 0.14$ was rather symmetrical, although not the same as that of Tonkin *et al.* (2003), as can be seen in Fig. 14(b), Fig. 16(c)
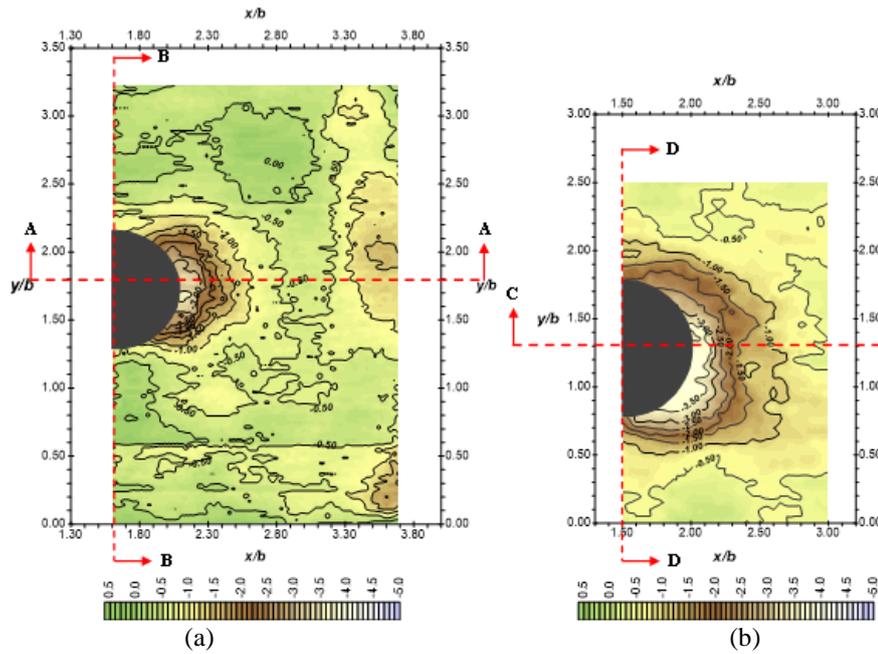
Fig. 15. Scour around the vertical cylinder. (a) *b/B* = 0.25 (present experiment) and (b) *b/B* = 0.14 (Kuswandi *et al.*, 2017).
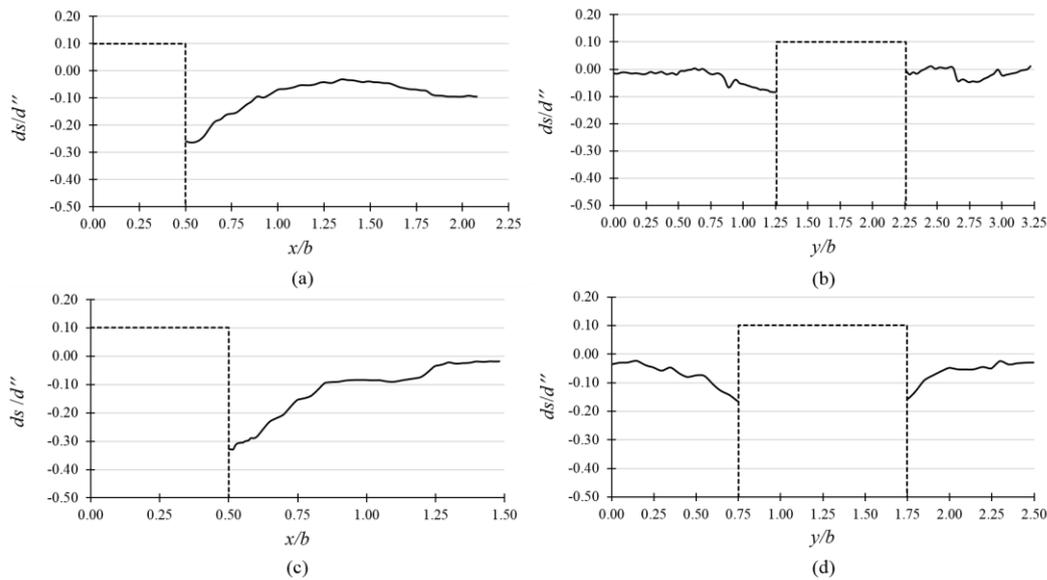
Fig. 16. Cross sections of local scour (a) along A-A, (b) along B-B, *b/B* = 0.25 (present experiment) and (c) along C-C and (d) along D-D for *b/B* =0.14 (Kuswandi *et al.*, 2017).

and Fig. 16(d). The maximum scour depth in Kuswandi *et al.* (2017) was 0.35 *d″*, which is closer to that of Tonkin *et al.* (2003).

4. CONCLUSION

The dam break system can be used to simulate tsunami run up on land. The ratio between d_0-d_3 and *L* affects the run-up height and duration. Thus, such a ratio should be considered when simulating tsunami based on a dam break system. The run-up height was lower than the analytical solution for an unlimited upstream reservoir length and followed

Eq. (8). Since ξ is normally very small, a real tsunami breaking at a coastal area is likely to be more similar to a dam break surge rather than to a solitary wave.

The two-gate dam break system may be used to simulate different tsunami lengths. An additional gate can be used to reduce or remove entirely the unwanted secondary run-up, which make this simulation of the run-down uninterrupted by the secondary run-up caused by upstream wall reflection. The dam break system generated run-up and run-down velocity patterns were similar to those of solitary waves.

A relatively small dam break model can be used to simulate local scouring around a vertical cylinder. However the scouring depth was relatively small but sufficient for an observation. The scour pattern around the vertical cylinder at $b/B = 0.25$ was not symmetrical due to flow separation of high Froude number at the cylinder location. The scour pattern at $b/B = 0.14$ was more symmetrical as the effect of flow separation reduced.

In the future, the study will be extended to investigate run-up and run-down for various slopes. The facility will also be used to simulate tsunami run-ups and tsunami overflow of seawall structures more accurately, especially during the run-down with the absence of the secondary run-ups due reflection from the upstream wall. It is expected that a mitigation technique to strengthen seawalls against scouring and toppling may be studied using such a facility.

ACKNOWLEDGEMENTS

REFERENCES

Aureli, F., S. Dazzi, A. Maranzoni, P. Mignosa, R. Vacondio (2015). Experimental and numerical evaluation of the force due to the impact of a dam break wave on a structure. *Advances in Water Resources* 76, 29-42.

Chanson, H. (2005). *Applications of the Saint-Venant equations and method of characteristics to the dam break Wave Problem.* The University of Queensland, St Lucia.

Crespo, A. J. C., J. M. Domínguez, B. D. Rogers, M. Gómez-Gesteira, S. Longshaw, R. Canelas, R. Vacondio, A. Barreiro and O. García-Feal (2015). DualSPHysics:Open source parallel CFD solver base on Smoothed Particle Hydrodynamics (SPH). *Computer Physics Communications* 187, 204–216.

Crespo, A. J. C., M. Gómez-Gesteira, and R. A. Dalrymple (2008). Modeling Dam Break Behavior over a Wet Bed by a SPH Technique. *Journal of Waterway, Port, Coastal, and Ocean Engineering* 134(6), 313-320.

Dal, K., S. Evangelista, A. Yilmaz and S. Kocaman (2017). Validation of Dam-Break Problem over Dry Bed using SPH. *International Journal of Advanced Engineering Research and Science (IJAERS)* 4(12), 209-2013**.**

Dalrymple, R. A. and D. L. Kriebel (2005). Lessons in Engineering from the Tsunami in Thailand. *The Bridge* 35(2).

Francis, M. J. (2006). Tsunami Inundation Scour Of Roadways, Bridges And Foundations. Observations And Technical Guidance from The Great Sumatra Andaman Tsunami. *EERI/FEMA NEHRP Professional Fellowship Report.*

Kato, F., S. Sato and H. Yeh (2000). Large-scale experiment on dynamic response of sand bed around a cylinder due to tsunami. *International Journal Coastal Engineering* 1848-1859.

Kuswandi, R. Triatmadja, Istiarto (2017). Simulation of Scouring Around A Vertical Cylinder Due To Tsunami. *Science of Tsunami Hazard* 36(2), 59-69.

Liu, G. R. and M. B. Liu (2003). *Smoothed Particle Hydrodynamics, a messfree particle method.* World Scientific Publishing Co. Pte. Ltd.

Lucy. L. B. (1977). A numerical approach to the testing of the fission hypothesis. *Astronomical Journal* 82, 1013–1024.

Mas, E., A. Suppasri, F. Imamura and S. Koshimura (2012). Agent-based Simulation of the 2011 Great East Japan Earthquake/Tsunami Evacuation: An Integrated Model of Tsunami Inundation and Evacuation. *International Journal of Natural Disaster Science* 34(1), 41-57.

Monaghan, J. J. and J. C. Lattanzio (1985). A refined particle method for astrophysical problems. *Journal of Astronomy and Astrophysics* 145, 135-143

Panalaran S., R. Triatmadja, and B. S. Wignyosukarto (2016, July). Mathematical modeling of wave forces on cylinders group using DualSPHysics. In *AIP Conference Proceedings* 1755, 060004.

Synolakis, C. E. (1987). The run-up of solitary waves. *International Journal of Fluid Mechanics* 185, 523-546.

Tonkin, P. Susan, Harry Yeh, Fuminori Kato, and Shinji Sato (2003). Tsunami scour around a cylinder. *International Journal Fluid Mechanics* 496, 165-192.

Triatmadja, R. and A. Nurhasanah (2012). Tsunami force on buildings with openings and protection. *International Journal of Earthquake and Tsunami* 6(4), 125-142.

Triatmadja, R., S. N. Hijah and A. Nurhasanah (2011). Scouring around coastal structures due to tsunami surge. *Proceedings in 6th Annual International Workshop & Expo on Sumatera Tsunami Disaster & Recovery 2011 in Conjuction with 4th South China Sea Tsunami Workshop.*TS 3-18.

Vallée, M. (2007). Rupture properties of the giant Sumatra earthquake imaged by empirical

green's function analysis. *Bulletin of the Seismological Society of America* 97(1A).

Wang, X. and Philip L. F. Liu (2006). An analysis of 2004 Sumatra earthquake fault plane mechanisms and Indian Ocean tsunami. *International Journal of Hydraulic Research* 44(2), 147–154.

Widjo, K. (2011). *South Java Tsunami Model Using Highly Resolved Data and Probable Tsunamigenic Sources*. Ph.D. thesis, Fakultät für Bauingenierurwesen und geodäsie der Gottfried Wilhelm Leibniz Unversität Hannover.

Xu. X. (2016). An improved SPH approach for simulating 3D dam break flows with breaking waves. *Computer Methods Applied Mechanical Engineering* 311,723–742.